

Enhanced spectral profile in the study of Doppler-broadened Rydberg atoms

Bo-Han Wu¹, Ya-Wen Chuang¹, Yi-Hsin Chen^{1,+}, Jr-Chiun Yu¹, Ming-Shien Chang², and Ite A. Yu^{1,*}

¹Department of Physics and Frontier Research Center on Fundamental and Applied Sciences of Matters, National Tsing Hua University, Hsinchu 30013, Taiwan

²Institute of Atomic and Molecular Sciences, Academia Sinica, Taipei 10617, Taiwan

+Corresponding author: yhchen920@gmail.com

*Corresponding author: yu@phys.nthu.edu.tw

ABSTRACT

Combination of the electromagnetically-induced-transparency (EIT) effect and Rydberg-state atoms has attracted great attention recently due to its potential application in the photon-photon interaction or qubit operation. In this work, we studied the Rydberg-EIT spectra with room-temperature ⁸⁷Rb atoms. Spectroscopic data under various experimental parameters all showed that the contrast of EIT transparency as a function of the probe intensity is initially enhanced, reaches a maximum value and then decays gradually. The contrast of spectral profile at the optimum probe field intensity is enhanced by 2–4 times as compared with that at weak intensity. Moreover, the signal-to-noise ratio of the spectrum can potentially be improved by 1 or 2 order of magnitude. We provided a theoretical model to explain this behavior and clarified its underlying mechanism. Our work overcomes the obstacle of weak signal in the Rydberg-EIT spectrum caused by an apparent relaxation rate of the Rydberg polariton and weak coupling transition strength, and provides the useful knowledge for the Rydberg-EIT study.

Introduction

Rydberg atom has become a popular research topic in recent decades, especially in the context of quantum information science, thanks to its physical properties. The weak dipole transition between ground and highly-excited Rydberg states prolongs the lifetime of Rydberg atoms^{1,2}. The large polarizability of Rydberg atoms gives rise to strong long-range interactions. It would couple the nearby atoms strongly through the immense dipole-dipole interaction. The strong interaction between Rydberg atoms leads to a blockade effect, implying a double excitation for a distance smaller than the blockade radius is strongly suppressed^{3–6}. With the unique features of above, Rydberg atom is a good candidate for the demonstration of novel quantum devices, such as single-photon transistors^{7,8} as well as quantum phase gate^{9–11}, single-photon sources^{12–14}, and quantum simulator¹⁵.

Electromagnetically-induced-transparency (EIT) spectrum provides the direct nondissipative optical detections of Rydberg energy levels, atom-atom interaction, and wall-atom interaction in a thin cell^{16–20}. An additional microwave field can break the symmetry of Rydberg-EIT interference, making it a good way to precisely determine the electric field of the microwave²¹. Besides the EIT spectra, the quantum information carried by photons can be dynamically encoded in Rydberg polaritons, allowing for storage, control, and retrieval of quantum states^{22,23}. To perform the above mentioned studies with Rydberg-state atoms, it is necessary to lock laser frequencies to a two-photon transition frequency. The EIT spectrum provides a convenient way to stabilize the laser frequencies for the studies²⁴.

We carried out our study in a room-temperature ⁸⁷Rb atomic vapor and investigated the Rydberg EIT spectra in this paper. The EIT peak height, i.e. the difference between the probe transmission at the EIT peak and that in the absence of the EIT effect, has been enhanced by 2–4 times at the optimum probe intensity as compared with that at weak probe intensity. Remarkably, the optimum intensity is influenced very little by the light polarization, orbitals of Rydberg state, and the principal quantum number of Rydberg state, n . We will provide a theoretical model for the observed behavior of the EIT peak height as a function of the probe intensity. In addition, when one applies a stronger probe intensity or power in the measurement, the signal level of the probe field is immediately enhanced. Thus, as for dominant noise being not caused by fluctuation of the probe power or intensity (but being caused by, for examples, stray light, electronic noise, detector's dark current, etc.), the signal-to-noise ratio (S/N) can be significantly improved. On the other hand, the spectral linewidth increases only by 2 folds. Therefore, the comprehensive feature of EIT effect leads to a better way for locking the upper transition frequency through a high contrast of the Rydberg-EIT spectrum, making it useful for the Rydberg-relevant researches.

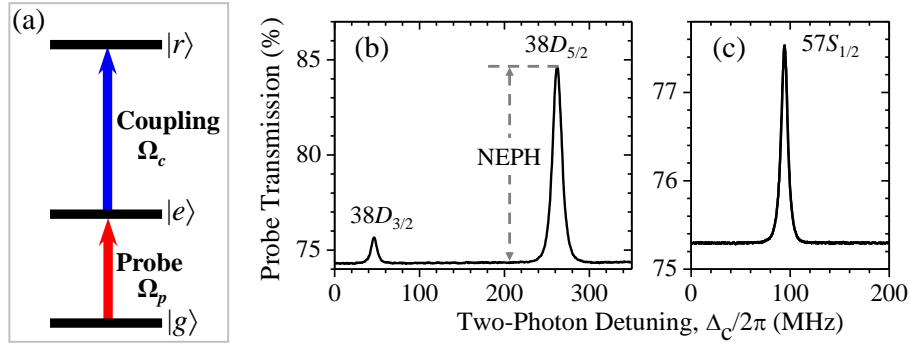


Figure 1. (a) Rydberg-EIT transition scheme. $|g\rangle$ is the ground state $|5S_{1/2}, F = 2\rangle$; $|e\rangle$ is the intermediate state $|5P_{3/2}, F' = 3\rangle$; and $|r\rangle$ is the Rydberg state $|nS\rangle$ or $|nD\rangle$ according to the experimental measurement. (b) and (c) Rydberg-EIT spectra. The coupling field frequency was swept across the transitions of $|5P_{3/2}, F' = 3\rangle$ to $|38D_{3/2}, F'' = 2, 3\rangle$ and $|38D_{5/2}, F'' = 2, 3, 4\rangle$ in (b), and across the transition of that to $|57S_{1/2}, F = 2\rangle$ state in (c), while the probe field frequency was fixed. In (b), we provide the definition of the normalized EIT peak height (NEPH), which is the difference between the transmissions of EIT peak and baseline. The intensities of the probe and coupling fields were 0.029 and 18 W/cm², respectively. Both light fields had the same polarization σ_+ in (b); and the probe field was σ_- polarized and coupling field was σ_+ polarized in (c). The values of NEPH are 0.014, 0.10, and 0.022 from left to right peaks in (b) and (c).

Results and Discussion

Experimental Observation

Rydberg EIT has a cascade-type (Ξ -type) level structure, which consists of a ground state, an intermediate excited state, and a Rydberg state, as shown in Fig. 1(a). The probe field couples the ground state $|5S_{1/2}, F = 2\rangle \equiv |g\rangle$ and the intermediate state $|5P_{3/2}, F' = 3\rangle \equiv |e\rangle$, while the coupling field drives the transition of $|e\rangle$ to Rydberg state $|r\rangle$. For each EIT spectrum measurement, we kept the probe field frequency resonant to $|g\rangle$ - $|e\rangle$ transition, while the frequency of the coupling field was swept across the $|e\rangle$ - $|r\rangle$ transition. The probe field has the maximum transmission when the two light fields are resonant to the Rydberg state due to the quantum interference of EIT effect. Figures 1(b) and 1(c) show the typical Rydberg-EIT spectra. Far from resonance, atoms in the excited state are less likely pumped to the Rydberg state. It can be viewed as a two-level transition, resulting a high absorption. Here, we define the normalized EIT peak height (NEPH) as the transmission difference between EIT and two-level transitions. The values of NEPH are 0.014, 0.10, and 0.022 from left to right peaks in Figs. 1(b) and 1(c).

To systematically study the NEPH, we varied the intensities of the probe and coupling fields, the Rydberg states, and the light polarization configurations for different orbitals of Rydberg state. As shown in Fig. 2, a stronger Ω_c (with fixed Rydberg state of $|38D_{5/2}\rangle$) or a lower Rydberg state (with fixed coupling intensity of 18 W/cm²) leads to a greater NEPH. Note that the intensity of the coupling or probe field specified in this article is the intensity at the center of the Gaussian beam profile of the laser field. The phenomenon can be explained by the expression of EIT transmission $T \sim \text{Exp}[-2\alpha\gamma/\Omega_c^2]$ under perturbation limit of the probe field, i.e. the Rabi frequency of probe field Ω_p is much weaker than that of the coupling field Ω_c ^{25,26}. Here α

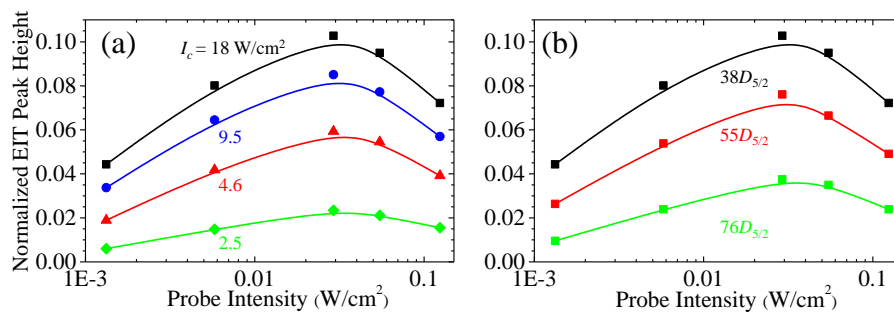


Figure 2. NEPH as a function of the intensity of the input probe field at (a) different intensities of the coupling field for the transition to Rydberg state of $|38D_{5/2}\rangle$ and (b) different principal quantum numbers of Rydberg states for the coupling intensity of 18 W/cm². Both measurements have the same polarization configuration of $\sigma_+ - \sigma_+$. The coupling intensities in units of W/cm² in (a) and selected Rydberg states in (b) are shown in the legends. Solid lines are the curves to guide the eye.

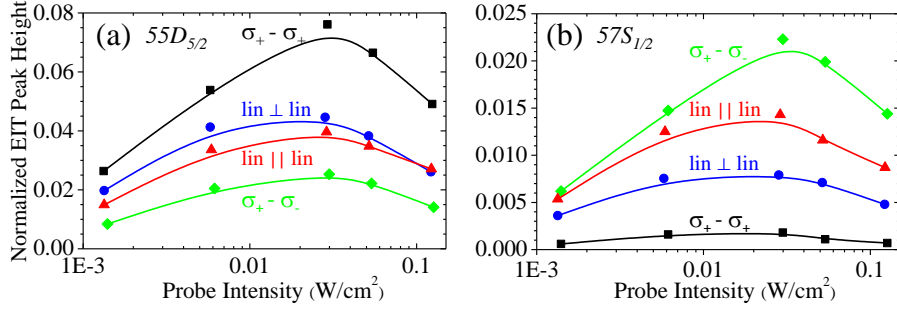


Figure 3. NEPH as a function of the intensity of the input probe field at different polarization configurations and Rydberg states, shown in the legends. The coupling intensity was 18 W/cm^2 in the both measurements. Solid lines are the curves to guide the eye.

is the optical density of the medium, γ is the decoherence rate between Rydberg and ground states, and Γ is the spontaneous decay rate of the intermediate state. The coupling Rabi frequency Ω_c is proportional to a power law $n^{*-3/2}$, where n^* is the effective principal quantum number of Rydberg state (see Method). The coupling strength between a higher Rydberg state and the intermediate state is weaker, resulting in a smaller Ω_c . The expression shows that a stronger Ω_c leads to a higher transmission of the probe field, which can qualitatively describe the data.

Besides, the polarization configurations of the laser fields were adjusted as $\sigma_+ - \sigma_+$, $\text{lin} \perp \text{lin}$, $\text{lin} \parallel \text{lin}$, and $\sigma_+ - \sigma_-$ by the half- or quarter-wave plates. For $|nD_{5/2}\rangle$ Rydberg state, the best polarization configuration is $\sigma_+ - \sigma_+$ (Fig. 3(a)). The hyperfine levels $F'' = 2, 3, 4$ of $|nD_{5/2}\rangle$ state are not resolvable so that all transition channels among the Hyperfine states and their Zeeman sub-levels need to be taken into account. The Zeeman state transition $|F' = 3, m'_F = 3\rangle$ to $|F'' = 4, m''_F = 4\rangle$ is a cycling transition, leading to a larger effective Ω_c . On the contrary, when the coupling field couples to $|nS_{1/2}\rangle$ Rydberg state, the polarization of $\sigma_+ - \sigma_-$ is the best configuration shown in Fig. 3(b). For $|nS_{1/2}\rangle$ state, only the excitation to $F'' = 2$ hyperfine state is allowed. For example, in the polarization configuration of $\sigma_+ - \sigma_+$ there are some probe excitations do not couple with the coupling field and, hence, the EIT transmission is reduced. Therefore, in order to get the best EIT contrast for a given $|nS\rangle$ or $|nD\rangle$ state, one should well select the best light polarization.

For each light polarization configuration or each Rydberg state, n , as well as the orbital, S or D , of Rydberg state, the Rabi frequencies of light shall be modified by averaging Clebsch-Gordan coefficients (CGC) among different hyperfine and Zeeman states. We define $\Omega_{p,0.1\text{W/cm}^2}$ as the Rabi frequency of the probe field with intensity of 0.1W/cm^2 and $\Omega_{p,0.1\text{W/cm}^2} = 2\pi \times 22.7$ MHz for each polarization of σ_+ , or σ_- , or π . The Rabi frequencies used in the measurements are summarized in Table 1. A detailed description of the derivation of Rabi frequencies can be found in Method. From the measurements of Figs. 2 and 3 and the analysis of Rabi frequencies, a greater NEPH corresponding to a larger Ω_c is quantitative proved.

Moreover, all measured results reveal a universal phenomenon, that as we enlarged the probe field intensity, NEPH initially increased, then reached a maximum (around intensity of 0.03 W/cm^2), and finally decreased. The optimum probe power is about 20 times stronger than the weakest power used in the measurement so that the S/N of NEPH can be enhanced. In most of EIT-relevant studies, people typically applied a weak probe intensity or Rabi frequency ($\Omega_p \ll \Omega_c$) because EIT theories work well under the perturbation limit. To our knowledge, this rising phenomenon of NEPH is not presented in any article so far and promotes a further study in this paper. After the optimization of the probe intensity, the best NEPH is 2 – 4 times larger, and therefore, the overall S/N can have 1 – 2 order of magnitude enhancement. Qualitatively, such enhancement or the behavior of rising NEPH is universal, which is irrelative to the laser polarization, the coupling intensity, the orbital and principal quantum

Table 1. Estimated $\Omega_{c,p}/2\pi$ (in units of MHz) for the coupling intensity of 18 W/cm^2 and for the probe intensity of 0.1 W/cm^2 in different polarization configurations. We assume the populations are equally distributed among different degenerate Zeeman states of $|g\rangle$. In the final column, $\Omega_{c,p}$ with $\text{CGC}=1$ is present. $\Omega_{p,0.1\text{W/cm}^2}$ is shown in the final row.

| Transitions | $\sigma_+ - \sigma_+$ | $\text{lin} \perp \text{lin}$ | $\text{lin} \parallel \text{lin}$ | $\sigma_+ - \sigma_-$ | CGC = 1 |
|---|-----------------------|-------------------------------|-----------------------------------|-----------------------|---------|
| $ 5P_{3/2}, F' = 3\rangle$ to $ 38D_{5/2}\rangle$ | 5.1 | 3.9 | 4.2 | 2.6 | 5.7 |
| $ 5P_{3/2}, F' = 3\rangle$ to $ 55D_{5/2}\rangle$ | 2.9 | 2.2 | 2.4 | 1.5 | 3.2 |
| $ 5P_{3/2}, F' = 3\rangle$ to $ 57S_{1/2}\rangle$ | 0.20 | 0.49 | 0.69 | 0.82 | 1.7 |
| $ 5P_{3/2}, F' = 3\rangle$ to $ 76D_{5/2}\rangle$ | 1.8 | 1.4 | 1.5 | 0.90 | 2.0 |
| $ 5S_{1/2}, F = 2\rangle$ to $ 5P_{3/2}, F' = 3\rangle$ | 22.7 | 22.7 | 22.7 | 22.7 | 33.2 |

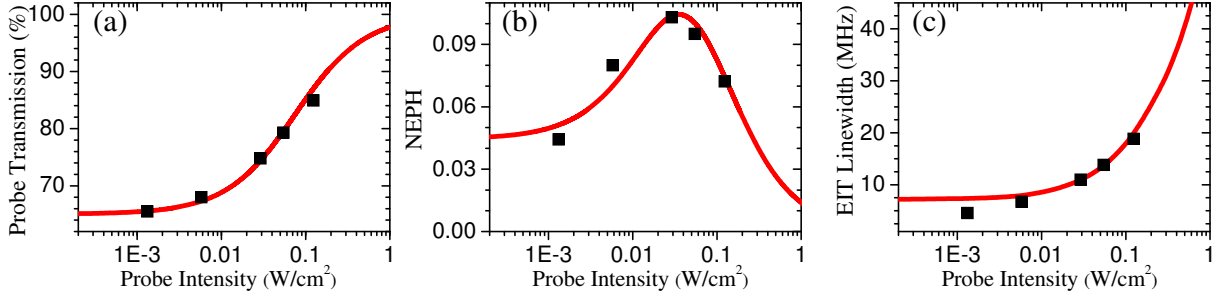


Figure 4. (a) Baseline transmission, i.e. the probe transmission at the coupling field frequency detuned far away from the two-photon resonance, (b) NEPH, and (c) linewidth, i.e. full width at half maximum, of the EIT profile versus the intensity of the input probe field. Black squares are the experimental data of the Rydberg state of $|38D_{5/2}\rangle$, and red lines are the theoretical predictions. The coupling intensity was 18 W/cm^2 , and two light fields were both σ_+ -polarized in the experimental measurement. We set $\Gamma_r = 2\pi \times 5 \text{ kHz}$ in the theoretical calculation. To fit the data well, $\alpha = 0.45$ and $(\Omega_{p,0.1\text{W/cm}^2}, \Omega_c, \gamma, \Gamma_e) = 2\pi \times (17.1, 4.5, 3.1, 18) \text{ MHz}$. We first determined α and the ratio of $\Omega_{p,0.1\text{W/cm}^2}$ to Γ_e by the fitting of (a). Then, the ratios of Ω_c and γ to Γ_e were resolved by the fitting of (b). Finally, we settled Γ_e by the fitting of (c).

number n of Rydberg state. The physics mechanism and criterion or experimental condition of the behavior will be discussed in the remaining part of the Results and Discussion.

Theoretical Model

We present the theoretical simulation by solving the optical Bloch equations (OBEs) and Maxwell-Schrödinger equation (MSE). According to the EIT theoretical studies^{27,28}, the spectrum or the dynamic behaviors in Doppler-broadened media can be simulated by a simple model used for Doppler-free media with the modifications of parameters, such as decoherence rate γ , optical depth α , and Rabi frequencies $\Omega_{c,p}$. Hence, the following equations are widely used in the EIT-relevant studies,

$$\partial_t \rho_{eg} = \frac{i}{2} [\Omega_p (\rho_{gg} - \rho_{ee}) + \Omega_c \rho_{rg}] - \frac{\Gamma_e}{2} \rho_{eg}, \quad (1a)$$

$$\partial_t \rho_{er} = \frac{i}{2} [\Omega_p \rho_{rg}^* + \Omega_c (\rho_{rr} - \rho_{ee})] - \left(\frac{\Gamma_e + \Gamma_r}{2} + i\Delta_c \right) \rho_{er}, \quad (1b)$$

$$\partial_t \rho_{rg} = \frac{i}{2} (\Omega_c^* \rho_{eg} - \Omega_p \rho_{er}^*) - (\gamma - i\Delta_c) \rho_{rg}, \quad (1c)$$

$$\partial_t \rho_{gg} = \frac{i}{2} (\Omega_p^* \rho_{eg} - \Omega_p \rho_{eg}^*) + \Gamma_e \rho_{ee}, \quad (1d)$$

$$\partial_t \rho_{rr} = \frac{i}{2} (\Omega_c^* \rho_{er} - \Omega_c \rho_{er}^*) - \Gamma_r \rho_{rr}, \quad (1e)$$

$$1 = \rho_{gg} + \rho_{ee} + \rho_{rr}, \quad (1f)$$

$$\left(\frac{1}{c} \partial_t + \partial_z \right) \Omega_p = i \frac{\alpha \Gamma_e}{2L} \rho_{eg}. \quad (1g)$$

Here ρ_{ij} is an element of the density-matrix operator of the three-level system, Δ_c is the detuning of the coupling field, Γ_e and Γ_r are the linewidths or the spontaneous decay rates of the intermediate state and Rydberg state, and L is the length of the medium.

We will describe how the predictions from above theoretical model can be consistent with the data. We first determine the optical density of the medium α and the ratio of $\Omega_{p,0.1\text{W/cm}^2}$ to Γ_e by numerically fitting the data of the probe transmission at the coupling frequency detuned far away from the two-photon resonance versus the intensity of the input probe, as shown in Fig. 4(a). The transmission at small values of Ω_p determines the value of optical density mainly. As Ω_p gets larger, the power broadening effect, indicated by Ω_p^2/Γ_e^2 , influences the increment of the transmission. Hence, the best fit gives the optical depth $\alpha = 0.45$ and $\Omega_{p,0.1\text{W/cm}^2}/\Gamma_e = 0.95$. Next, we fix $\Gamma_r = 2\pi \times 5 \text{ kHz}$, which is the spontaneous decay rate of $38D_{5/2}$ ²⁹, in the calculation of the NEPH predictions (Fig. 4(b)). The ratios of Ω_c and γ to Γ_e were resolved by the fitting because both of Ω_c and γ can affect the EIT peak height. This can be realized from the EIT peak transmission $T \sim \text{Exp}[-2\alpha(\gamma/\Gamma_e)/(\Omega_c/\Gamma_e)^2]$ under perturbation limit of the probe field^{25,26}. In addition, as all the frequency-related quantities, Ω_p , Ω_c , γ , etc., are normalized to or divided by Γ_e in Eq. (1), the calculation result becomes invariant with respect to Γ_e . Therefore, the NEPH can determine

Ω_c/Γ_e (or γ/Γ_e) but not Ω_c and Γ_e (or γ and Γ_e) individually. The actual value of Γ_e in units of MHz was derived by matching the theoretical EIT linewidths to the experimental ones as illustrated in Fig. 4(c). The three kinds of data shown in Figs. 4(a), 4(b), and 4(c) can uniquely determine a set of $\alpha = 0.45$ and $(\Omega_{p,0.1\text{W/cm}^2}, \Omega_c, \gamma, \Gamma_e) = 2\pi \times (17.1, 4.5, 3.1, 18)$ MHz.

The best fit of EIT spectra gives $\Gamma_e = 2\pi \times 18$ MHz, indicating that only a small fraction of room-temperature atoms interacts with the probe field. Note that the actual angular natural linewidth of the intermediate state $|e\rangle$ is $\Gamma = 2\pi \times 6$ MHz. In each measurement of the EIT spectrum, we kept the probe field frequency fixed at the resonant frequency of the transition from $|5S_{1/2}, F=2\rangle$ to $|5P_{3/2}, F'=3\rangle$, and swept the coupling field frequency. Atoms with high velocities v do not interact with the probe field at all due to the Doppler shift kv being large, where k is the wave vector of the probe light. Because the EIT scheme is formed by the cascade- or ladder-type transitions, no interaction with the probe field also means no influence from the coupling field. Only the atoms with low velocities can interact with the probe field and, consequently, also be influenced by the coupling field. In the lab frame, these atoms with low but non-zero velocities possess different resonance frequencies of the transition. A distribution of resonance frequencies, arising from the atoms with various velocities distributed around $v = 0$, can equivalently be seen as the broadening of the excited-state linewidth in the theoretical model treating all atoms with $v = 0$. Therefore, Γ_e of $2\pi \times 18$ MHz indicates that only the atoms, with $|kv|$ less than approximately $2\pi \times 9$ MHz, interacted with the probe and coupling fields and participated in the measurements.

The EIT linewidth is predominately determined by the coupling field intensity and optical density of the medium at the weak probe field regime. Employing room-temperature or hot atomic media, one typically applies a strong coupling field to diminish the influence of non-negligible decoherence rate γ on the EIT transmission. For a strong probe field, the power broadening effect occurs, resulting in the spectral width becomes broader. The linewidth at the optimum probe intensity, shown in Fig. 4(c), is only twice broader than that at weak intensity. As discussed before, the overall S/N of EIT peak can have 1–2 order of magnitude enhancement. The EIT dispersion, i.e. the slope of a frequency-modulated EIT spectrum, becomes much larger. If the probe field is further stronger, the increment of EIT linewidth and the decrement of NEPH becomes fast. The EIT spectrum doesn't benefit the Rydberg studies relied on the optical frequency lock.

NEPH Behavior

We now discuss the universal phenomena, that NEPH increases initially with weak Ω_p regime and then decreases at strong Ω_p regime. The theoretical model for Doppler-free atoms with effective parameters can phenomenologically describe the Doppler-broadened atomic medium well. Hence, in the following discussion, we will utilize this model to explain the observed behavior of NEPH. For simplicity, we start from the analysis of the absorption cross sections, which is equal to $\sigma_0 \times \text{Im}[\rho_{eg}\Gamma_e/\Omega_p]$, where σ_0 is the resonant absorption cross section under perturbation limit of the probe field. We define σ_{TL} as the absorption cross section of the baseline in a spectrum, which is resulted from the resonant transition in the two-level system. σ_{EIT} is defined as the absorption cross section of the EIT peak. Based on the steady-state solution of the optical-Bloch equations, we derive σ_{TL} and σ_{EIT} under the assumptions of $\Gamma_r \ll \Gamma_e$ and $\Gamma_r\Gamma_e \ll \Omega_c^2$ as

$$\frac{\sigma_{TL}}{\sigma_0} = \frac{\Gamma_e^2}{2\Omega_p^2 + \Gamma_e^2}, \quad \frac{\sigma_{EIT}}{\sigma_0} = \frac{\Gamma_e^2(2\gamma\Omega_c^2 + \Gamma_r\Omega_p^2)}{\Gamma_e\Omega_c^2(\Omega_c^2 + 2\gamma\Gamma_e) + \Omega_p^2(6\gamma\Omega_c^2 + \Gamma_e\Omega_c^2 + 2\Gamma_r\Omega_p^2)}. \quad (2)$$

The analysis of absorption cross section as well as the probe transmission will be discussed in two regimes: weak and strong Ω_p regimes. In the weak Ω_p regime, we further assume $\Omega_p^2 \ll \Gamma_e^2, \Omega_c^2$ and $\Gamma_r\Omega_p^2 \ll \Gamma_e\Omega_c^2$. The absorption cross sections of two-level and Rydberg-EIT systems can be expanded as

$$\frac{\sigma_{TL}}{\sigma_0} \approx 1 - \frac{2\Omega_p^2}{\Gamma_e^2}, \quad \frac{\sigma_{EIT}}{\sigma_0} \approx \frac{2\gamma\Gamma_e}{2\gamma\Gamma_e + \Omega_c^2} - \frac{2\Omega_p^2\gamma(6\gamma + \Gamma_e)}{(\Omega_c^2 + 2\gamma\Gamma_e)^2}, \quad \Delta\sigma = \sigma_{TL} - \sigma_{EIT} = A_1 + \frac{2B_1\Omega_p^2}{\Gamma_e^2}, \quad (3)$$

where

$$B_1 = \frac{\gamma\Gamma_e^2(2\gamma + \Gamma_e) - \Omega_c^2(4\gamma\Gamma_e + \Omega_c^2)}{(\Omega_c^2 + 2\gamma\Gamma_e)^2}.$$

If B_1 is positive, $\Delta\sigma$ as well as NEPH increases with increasing Ω_p . In the physical explanation, on one hand, the transmission of the probe field under the two-level transition slightly increases as increasing Ω_p due to the power broadening effect. On the other hand, in the EIT transition, a highly-excited Rydberg state can be treated as a meta-stable state because of the slow spontaneous decay rate. A strong Ω_p results in more populations to be driven into the excited state $|e\rangle$ and Rydberg state $|r\rangle$. According to EIT theory, the population ratio of $|r\rangle$ to $|g\rangle$ is determined by the ratio of Ω_p^2 to Ω_c^2 , and, thus, the population ratio becomes larger as Ω_p^2 increases under fixed Ω_c^2 . The less population in the ground state leads to a higher transmittance of the probe field. With a weak Ω_c , the rising transmittance for EIT transition would be faster than that for two-level transition. The initially-rising phenomenon in the data of NEPH versus the probe intensity can occur under $B_1 > 0$

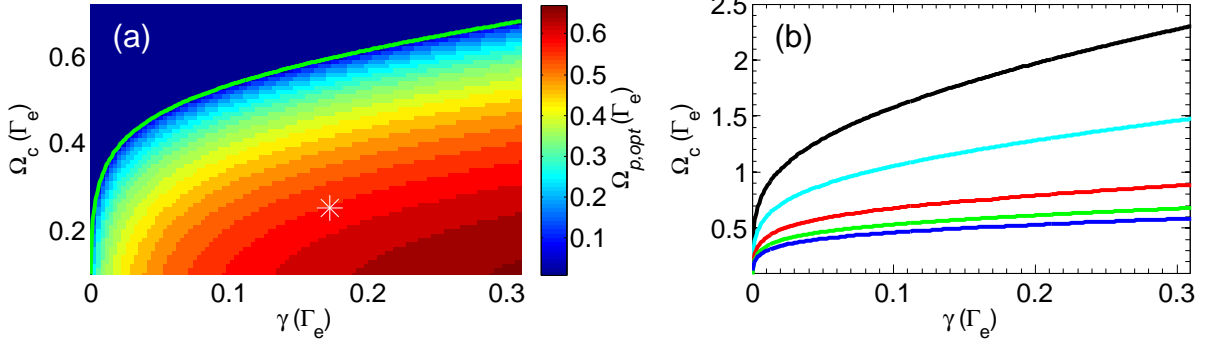


Figure 5. Panel (a) shows the simulation results of $\Omega_{p,opt}$ under a given set of Ω_c and γ , where $\Omega_{p,opt}$ is the probe Rabi frequency making NEPH reach the maximum value. OD is set as 0.45 for the calculation. The green solid line represents the boundary between zero and positive values of $\Omega_{p,opt}$. The marker * shows the experimental condition of Fig. 4. (b) Boundary lines for different optical densities. From top to bottom, ODs are 3 (black), 2 (cyan), 1 (red), 0.45 (green), and 0.1 (blue).

We now intend to explain the decreasing behavior at stronger Ω_p regime. Here, we assume $\Omega_p^2 \gg \Gamma_e^2, \Omega_c^2$. σ_{TL} and σ_{EIT} are presented as

$$\frac{\sigma_{TL}}{\sigma_0} \approx \frac{\Gamma_e^2}{2\Omega_p^2}, \quad \frac{\sigma_{EIT}}{\sigma_0} \approx \frac{\Gamma_e^2 (2\gamma\Omega_c^2 + \Gamma_r\Omega_p^2)}{\Omega_p^2 [(6\gamma + \Gamma_e)\Omega_c^2 + 2\Gamma_r\Omega_p^2]}, \quad \Delta\sigma = \sigma_{TL} - \sigma_{EIT} = \frac{A_2\Gamma_e^2}{2\Omega_p^2}, \quad (4)$$

where

$$A_2 = \frac{(2\gamma + \Gamma_e)\Omega_c^2}{(6\gamma + \Gamma_e)\Omega_c^2 + 2\Gamma_r\Omega_p^2}.$$

A_2 is always larger than zero, implying that $\Delta\sigma$ as well as NEPH decreases with increasing Ω_p . At a large Ω_p , the EIT peak transmission becomes saturated and has a little room for improvement, while the baseline transmission can still be significantly increased. Consequently, increment of the probe Rabi frequency makes the baseline transmission approach to the EIT peak transmission, implying the NEPH decreases to zero. The above argument is supported by $\Delta\sigma$ decreasing monotonically with Ω_p as shown by Eq. (4). Since NEPH initially increases at small Ω_p and finally decreases at large Ω_p , there must exist an optimum probe Rabi frequency, $\Omega_{p,opt}$, which makes NEPH reach its maximum value.

To observe the phenomenon that NEPH as a function of the probe intensity initially increases, then reaches a maximum, and eventually decreases to zero, B_1 must be positive. The condition $\Omega_c^2 \leq \Gamma_e (\sqrt{6\gamma^2 + \Gamma_e\gamma} - 2\gamma)$ makes $B_1 > 0$. In the numerical calculation with a given set of Ω_c and γ , we search for the optimal probe Rabi frequency, $\Omega_{p,opt}$, as shown in Fig. 5(a). The solid line sets the boundary in the parameter space between regions with zero and positive $\Omega_{p,opt}$. The experimental condition of the measurements in Fig. 4 were far from the border line, shown as * in the contour plot. Note that for a sufficient small optical density, e.g. $OD < 0.1$, the border line (blue line in Fig. 5(b)) well fits the above-mentioned condition. As the OD gets larger, the increasing NEPH phenomenon is within reach for a sufficient weak Ω_c , as shown in Fig. 5(b). Generally, the enhancement of EIT contrast or the increasing phenomenon of NEPH can be observed in the Λ -EIT or Rydberg-EIT systems with Doppler-broadened atoms or with cold atoms under an apparent decoherence rate^{27,28}.

Conclusion

We systematically investigated the best contrast of EIT peak in different polarization configurations of light fields, laser intensities, and orbitals and principal quantum numbers of Rydberg states. From the measurements and the analysis of Rabi frequencies, a greater NEPH corresponding to a larger Ω_c is quantitative proved. In addition, a universal phenomenon was experimentally observed that the EIT contrast increasing with the probe intensity and then decreasing for further stronger light field. The EIT contrast is enhanced by 2 – 4 times at the optimum probe field intensity as compared with that at weak intensity. Meanwhile, the signal-to-noise ratio of the profile can be improved by 1 or 2 order of magnitude. The enhancement can be achieved in most of the Λ -EIT or Rydberg-EIT experiments using Doppler-broadened atoms or using cold atoms under an apparent decoherence rate. Without considering the Doppler effect due to the atomic motion, the thermal Rydberg-EIT spectrum can be predicted by using the simulation for a Doppler-free medium with the modification of parameters. The theoretical model

can well fit the data and simulate the rising behavior of NEPH. Our studies provide a better way of locking the upper transition frequency through a high contrast Rydberg-EIT spectrum and advances the Rydberg-atom-relevant studies.

Methods

Setup and Measurements

The probe field couples $|g\rangle$ and $|e\rangle$ states with wavelength of 780 nm, generated from an external cavity diode laser. The coupling field drives atoms from $|e\rangle$ to $|r\rangle$ states with wavelength of 480 nm, produced from a frequency doubled diode laser system (Toptica TA SHG pro). These two beams are sent into a counter-propagation direction to diminish the Doppler effect due to the atomic motion. We applied a dichroic mirror (DM) to separate the mixed probe field from the coupling beam after the vapor cell. The full width at e^{-2} maximum of the probe and coupling beams were 1.4 mm and 2.2 mm, respectively. The vapor cell is filled with the admixture of ^{87}Rb and ^{85}Rb atoms at the temperature of 300 K.

Deviation of Table 1

Considering the equivalent CGC^{30,31}, the Rabi frequency is derived as a function of laser intensity,

$$\Omega_p = \langle a_p \rangle \Gamma \sqrt{\frac{I_p}{2I_{sat}}}, \quad \Omega_c = \frac{ea_0}{\hbar} C_{S,D} \langle a_c \rangle \sqrt{\frac{2I_c}{c\epsilon_0}} n^{*-\frac{3}{2}}, \quad (5)$$

where $\langle a_p \rangle = \sqrt{\sum_i P_i C_{p,i}^2}$ and $\langle a_c \rangle = \sqrt{\sum_i P_i C_{p,i}^2 C_{c,i}^2 / \langle a_p \rangle^2}$. I_p and I_c are the laser intensities of probe and coupling fields, I_{sat} is the saturation intensity of the probe field transition. n^* is the effective principal quantum number of Rydberg state which replaces the true n with the relation of $n^* = n - \delta(n, l, j)$. The quantum defects $\delta(n, l, j)$ of ^{87}Rb atoms were measured by Mack et al.,³² and for $n > 20$ that are around 1.34(1) and 3.13 for $|nD_{3/2,5/2}\rangle$ and $|nS_{1/2}\rangle$ states, respectively. $C_S = 4.5$ and $C_D = 8.5$ for S and D orbitals of Rydberg state. In the expressions of $\langle a_p \rangle$ and $\langle a_c \rangle$, P_i represents the population in the i -th Zeeman ground state, $C_{p,i}$ and $C_{c,i}$ are the CGCs of the probe and coupling transitions for each subsystem.

The polarization configurations of the laser fields were adjusted as $\sigma_+ - \sigma_+$, $\text{lin} \perp \text{lin}$, $\text{lin} \parallel \text{lin}$, and $\sigma_+ - \sigma_-$ by the half- or quarter-wave plates. To derive the effective Ω_p , we consider all the transition channels among Zeeman states from $|5S_{1/2}, F = 2\rangle$ to $|5P_{3/2}, F' = 3\rangle$. The transition of σ_+ , or σ_- , or π polarizations of the probe field all gives $\langle a_p \rangle = \sqrt{7/15}$. The coupling field drives atoms from $|5P_{3/2}, F' = 3\rangle$ to $|nD_{5/2}, F'' = 2, 3, 4\rangle$ or $|nS_{1/2}, F'' = 2\rangle$. Note that the D state hyperfine levels are not resolvable, and hence all transition channels need to be taken into account. The values of $\Omega_{c,p}$ are summarized in Table 1.

Acknowledgements

This work received the support of the Ministry of Science and Technology of Taiwan under Grant Nos. 105-2119-M-007-004, 105-2923-M-007-002-MY3, and 105-2112-M-007-035-MY2. MSC acknowledges the Academia Sinica for equipment grant. BHW, MSC, and IAY acknowledge many fruitful discussions on this work under the platform sponsored by the Experimental Collaboration Program of National Center for Theoretical Science. All authors thank Dr. Bongjune Kim for comments, and Dr. Artūrs Ciniņš and Dr. Teodora Kirova for discussion.

Author Contributions Statement

I.A.Y. conceived the study and designed the experiment. Y.-W.C. measured the spectra supervised by M.-S.C. B.-H.W., Y.-H.C., and J.-C.Y. studied the theory and analyzed the data supervised by I.A.Y. B.-H.W. and Y.-H.C. made the figures and table. The manuscript was written by Y.-H.C. with the help from B.-H.W., I.A.Y., and M.-S.C.

Additional Information

The authors declare no competing financial interests.

References

1. Saffman, M., Walker, T. G. & Mølmer, K. Quantum information with rydberg atoms. *Rev. Mod. Phys.* **82**, 2313–2363 (2010). URL <http://link.aps.org/doi/10.1103/RevModPhys.82.2313>. DOI 10.1103/RevModPhys.82.2313.
2. Gallagher, T. F. Rydberg atoms. *Rep. Prog. Phys.* **51**, 143 (1988).

3. Comparat, D. & Pillet, P. Dipole blockade in a cold rydberg atomic sample. *J. Opt. Soc. Am. B* **27**, A208–A232 (2010). URL <http://josab.osa.org/abstract.cfm?URI=josab-27-6-A208>. DOI 10.1364/JOSAB.27.00A208.
4. Sevinçli, S. *et al.* Quantum interference in interacting three-level rydberg gases: coherent population trapping and electromagnetically induced transparency. *Journal of Physics B: Atomic, Molecular and Optical Physics* **44**, 184018 (2011). URL <http://stacks.iop.org/0953-4075/44/i=18/a=184018>.
5. Friedler, I., Petrosyan, D., Fleischhauer, M. & Kurizki, G. Long-range interactions and entanglement of slow single-photon pulses. *Phys. Rev. A* **72**, 043803 (2005). URL <http://link.aps.org/doi/10.1103/PhysRevA.72.043803>. DOI 10.1103/PhysRevA.72.043803.
6. Gorshkov, A. V., Otterbach, J., Fleischhauer, M., Pohl, T. & Lukin, M. D. Photon-photon interactions via rydberg blockade. *Phys. Rev. Lett.* **107**, 133602 (2011). URL <http://link.aps.org/doi/10.1103/PhysRevLett.107.133602>. DOI 10.1103/PhysRevLett.107.133602.
7. Tiarks, D., Baur, S., Schneider, K., Dürr, S. & Rempe, G. Single-photon transistor using a förster resonance. *Phys. Rev. Lett.* **113**, 053602 (2014). URL <http://link.aps.org/doi/10.1103/PhysRevLett.113.053602>. DOI 10.1103/PhysRevLett.113.053602.
8. Gorniaczyk, H., Tresp, C., Schmidt, J., Fedder, H. & Hofferberth, S. Single-photon transistor mediated by interstate rydberg interactions. *Phys. Rev. Lett.* **113**, 053601 (2014). URL <http://link.aps.org/doi/10.1103/PhysRevLett.113.053601>. DOI 10.1103/PhysRevLett.113.053601.
9. Isenhower, L. *et al.* Demonstration of a neutral atom controlled-not quantum gate. *Phys. Rev. Lett.* **104**, 010503 (2010). URL <http://link.aps.org/doi/10.1103/PhysRevLett.104.010503>. DOI 10.1103/PhysRevLett.104.010503.
10. Shahmoon, E., Kurizki, G., Fleischhauer, M. & Petrosyan, D. Strongly interacting photons in hollow-core waveguides. *Phys. Rev. A* **83**, 033806 (2011). URL <http://link.aps.org/doi/10.1103/PhysRevA.83.033806>. DOI 10.1103/PhysRevA.83.033806.
11. Tiarks, D., Schmidt, S., Rempe, G. & Dürr, S. Optical π phase shift created with a single-photon pulse. *Science Advances* **2** (2016). URL <http://advances.sciencemag.org/content/2/4/e1600036>. DOI 10.1126/sciadv.1600036. <http://advances.sciencemag.org/content/2/4/e1600036.full.pdf>.
12. Saffman, M. & Walker, T. G. Creating single-atom and single-photon sources from entangled atomic ensembles. *Phys. Rev. A* **66**, 065403 (2002). URL <http://link.aps.org/doi/10.1103/PhysRevA.66.065403>. DOI 10.1103/PhysRevA.66.065403.
13. Dudin, Y. O. & Kuzmich, A. Strongly interacting rydberg excitations of a cold atomic gas. *Science* **336**, 887–889 (2012). URL <http://www.sciencemag.org/content/336/6083/887.abstract>. DOI 10.1126/science.1217901.
14. Müller, M. M. *et al.* Room-temperature rydberg single-photon source. *Phys. Rev. A* **87**, 053412 (2013). URL <http://link.aps.org/doi/10.1103/PhysRevA.87.053412>. DOI 10.1103/PhysRevA.87.053412.
15. Weimer, H., Müller, M., Lesanovsky, I., Zoller, P. & Büchler, H. P. A rydberg quantum simulator. *Nat Phys* **6**, 382 (2010). URL <http://dx.doi.org/10.1038/nphys1614>. DOI 10.1038/nphys1614.
16. Mohapatra, A. K., Jackson, T. R. & Adams, C. S. Coherent optical detection of highly excited rydberg states using electromagnetically induced transparency. *Phys. Rev. Lett.* **98**, 113003 (2007). URL <http://link.aps.org/doi/10.1103/PhysRevLett.98.113003>. DOI 10.1103/PhysRevLett.98.113003.
17. Pritchard, J. D. *et al.* Cooperative atom-light interaction in a blockaded rydberg ensemble. *Phys. Rev. Lett.* **105**, 193603 (2010). URL <http://link.aps.org/doi/10.1103/PhysRevLett.105.193603>. DOI 10.1103/PhysRevLett.105.193603.
18. Kübler, H., Shaffer, J. P., Baluksian, T., Löw, R. & Pfau, T. Coherent excitation of rydberg atoms in micrometre-sized atomic vapour cells. *Nat Photon* **4**, 112–116 (2010). URL <http://dx.doi.org/10.1038/nphoton.2009.260>. DOI 10.1038/nphoton.2009.260.
19. Pritchard, J. D., Weatherill, K. J. & Adams, C. S. *NONLINEAR OPTICS USING COLD RYDBERG ATOMS*, 301 (WORLD SCIENTIFIC, 2013). URL http://www.worldscientific.com/doi/abs/10.1142/9789814440400_0008.
20. Löw, R. *et al.* An experimental and theoretical guide to strongly interacting rydberg gases. *Journal of Physics B: Atomic, Molecular and Optical Physics* **45**, 113001 (2012). URL <http://stacks.iop.org/0953-4075/45/i=11/a=113001>.

21. Sedlacek, J. A. *et al.* Microwave electrometry with rydberg atoms in a vapour cell using bright atomic resonances. *Nat Phys* **8**, 819 (2012). URL <http://dx.doi.org/10.1038/nphys2423>. DOI 10.1038/nphys2423.
22. Maxwell, D. *et al.* Storage and control of optical photons using rydberg polaritons. *Phys. Rev. Lett.* **110**, 103001 (2013). URL <http://link.aps.org/doi/10.1103/PhysRevLett.110.103001>. DOI 10.1103/PhysRevLett.110.103001.
23. Ripka, F., Chen, Y.-H., Löw, R. & Pfau, T. Rydberg polaritons in a thermal vapor. *Phys. Rev. A* **93**, 053429 (2016). URL <http://link.aps.org/doi/10.1103/PhysRevA.93.053429>. DOI 10.1103/PhysRevA.93.053429.
24. Abel, R. P. *et al.* Laser frequency stabilization to excited state transitions using electromagnetically induced transparency in a cascade system. *Applied Physics Letters* **94**, 071107 (2009). URL <http://dx.doi.org/10.1063/1.3086305>. DOI 10.1063/1.3086305. <http://dx.doi.org/10.1063/1.3086305>.
25. Fleischhauer, M., Imamoglu, A. & Marangos, J. P. Electromagnetically induced transparency: Optics in coherent media. *Rev. Mod. Phys.* **77**, 633–673 (2005). URL <http://link.aps.org/doi/10.1103/RevModPhys.77.633>. DOI 10.1103/RevModPhys.77.633.
26. Chen, Y.-F., Kao, Y.-M., Lin, W.-H. & Yu, I. A. Phase variation and shape distortion of light pulses in electromagnetically induced transparency media. *Phys. Rev. A* **74**, 063807 (2006). URL <http://link.aps.org/doi/10.1103/PhysRevA.74.063807>. DOI 10.1103/PhysRevA.74.063807.
27. Su, S.-W., Chen, Y.-H., Gou, S.-C. & Yu, I. A. An effective thermal-parametrization theory for the slow-light dynamics in a doppler-broadened electromagnetically induced transparency medium. *Journal of Physics B: Atomic, Molecular and Optical Physics* **44**, 165504 (2011). URL <http://stacks.iop.org/0953-4075/44/i=16/a=165504>.
28. Su, S.-W., Chen, Y.-H., Gou, S.-C., Horng, T.-L. & Yu, I. A. Dynamics of slow light and light storage in a doppler-broadened electromagnetically-induced-transparency medium: A numerical approach. *Phys. Rev. A* **83**, 013827 (2011). URL <http://link.aps.org/doi/10.1103/PhysRevA.83.013827>. DOI 10.1103/PhysRevA.83.013827.
29. Branden, D. B. *et al.* Radiative lifetime measurements of rubidium rydberg states. *Journal of Physics B: Atomic, Molecular and Optical Physics* **43**, 015002 (2010). URL <http://stacks.iop.org/0953-4075/43/i=1/a=015002>.
30. Guan, P.-C. & Yu, I. A. Simplification of the electromagnetically induced transparency system with degenerate zeeman states. *Phys. Rev. A* **76**, 033817 (2007). URL <http://link.aps.org/doi/10.1103/PhysRevA.76.033817>. DOI 10.1103/PhysRevA.76.033817.
31. Deiglmayr, J. *et al.* Coherent excitation of rydberg atoms in an ultracold gas. *Optics Communications* **264**, 293 – 298 (2006). URL <http://www.sciencedirect.com/science/article/pii/S0030401806004901>. DOI <http://dx.doi.org/10.1016/j.optcom.2006.02.058>. Quantum Control of Light and Matter In honor of the 70th birthday of Bruce Shore.
32. Mack, M. *et al.* Measurement of absolute transition frequencies of ^{87}Rb to nS and nD rydberg states by means of electromagnetically induced transparency. *Phys. Rev. A* **83**, 052515 (2011). URL <http://link.aps.org/doi/10.1103/PhysRevA.83.052515>. DOI 10.1103/PhysRevA.83.052515.